

Influence of induced axial magnetic field on plasma dynamics and radiative characteristics of Z pinches

V. L. Kantsyrev,¹ A. A. Esaulov,¹ A. S. Safronova,¹ A. L. Velikovich,² L. I. Rudakov,³ G. C. Osborne,¹
I. Shrestha,¹ M. E. Weller,¹ K. M. Williamson,^{1,4} A. Stafford,¹ and V. V. Shlyaptseva¹

¹*Physics Department, University of Nevada, Reno, Nevada 89557, USA*

²*Plasma Physics Division, Naval Research Laboratory, Washington, D.C. 20375*

³*Icarus Research Inc., Bethesda, Maryland 20824, USA*

⁴*Plasma Engineering Research Laboratory, Texas A&M University, Corpus Christi, TX 78412, USA*

(Received 18 April 2011; revised manuscript received 2 August 2011; published 21 October 2011)

The influence of an induced axial magnetic field on plasma dynamics and radiative characteristics of Z pinches is investigated. An axial magnetic field was induced in a novel Z-pinch load: a double planar wire array with skewed wires (DPWAsk), which represents a planar wire array in an open magnetic configuration. The induced axial magnetic field suppressed magneto-Rayleigh-Taylor (MRT) instabilities (with $m = 0$ and $m = 1$ instability modes) in the Z-pinch plasma. The influence of the initial axial magnetic field on the structure of the plasma column at stagnation was manifested through the formation of a more uniform plasma column compared to a standard double planar wire array (DPWA) load [V. L. Kantsyrev *et al.*, *Phys. Plasmas* **15**, 030704 (2008)]. The DPWAsk load is characterized by suppression of MRT instabilities and by the formation of the sub-keV radiation pulse that occurs before the main x-ray peak. Gradients in plasma parameters along the cathode-anode gap were observed and analyzed for DPWAsk loads made from low atomic number Z (Al) and mid-Z (brass) wires.

DOI: [10.1103/PhysRevE.84.046408](https://doi.org/10.1103/PhysRevE.84.046408)

PACS number(s): 52.59.Qy

I. INTRODUCTION

For inertial confinement fusion (ICF) and other potential applications based on Z-pinch-driven x-ray sources, it is necessary to improve our understanding of the basic physics and scaling of ablation dynamics, implosion dynamics, plasma heating mechanisms, and radiation performance of wire arrays during the stagnation phase. It is also important to evaluate the scaling of wire arrays to a more compact size and higher current, and to develop methods to shape the x-ray radiation pulse. Despite significant progress in the development of Z-pinch plasma radiation sources based on the implosions of single and nested cylindrical wire arrays [1], the design and testing of novel Z-pinch loads represent another approach to generating a well-controlled radiation source. Previous work done to improve Z-pinch radiation sources was highlighted in experiments with single planar wire arrays (SPWA) [2], double planar wire arrays (DPWA) [3], and triple planar wire arrays (TPWA) [4]. These compact PWAs are good candidates for novel compact multisource ICF hohlraum concepts [5].

The most intense and well-studied x-ray radiator at the 1.7 MA Zebra generator is a DPWA that consists of two parallel planar rows of wires [3,4]. This novel Z-pinch load is characterized by a combination of high total radiation yield (power >28 – 30 kJ/ >1 TW) in nanosecond-scale rise time bursts, small size (array width $D \sim 3$ – 6 mm and inter-row gap $\Delta \sim 1.5$ – 6 mm), and by the possibility of its usefulness in radiation pulse shaping [3,4,6]. Another important feature of the DPWA configuration is its easy diagnostic access for observing plasma implosion and stagnation; diagnostic lines of sight can be directed parallel to the wire rows, which allows for easier study of the precursor formation with both optical laser diagnostics and time-gated x-ray pinhole imagers [3,4,7]. Superiority in radiation performance of DPWA loads as well as an easy diagnostic access toward the central region of the load made the DPWA configuration a perfect candidate for the

introduction of an axial component to the magnetic field by modifying a DPWA load into a skewed wire DPWA (DPWAsk) configuration. This was done by leaning the wires of each plane into opposite directions from their original angles along the central Z-pinch axis (Fig. 1).

In early theoretical work, the possibility of using axial magnetic fields was considered as an effective method to reduce the growth of classical MRT instability modes [8–10]. Early proposed applications to this theory involve a scheme in which the wires of a cylindrical wire array are twisted along a curved surface [11] to create an initial axial magnetic field B_z and provide more effective control of x-ray generation. Similarly, the major expectation from novel DPWAsk load designs is to improve the radiation characteristics of the plasma by mitigating the MRT instabilities to reduce large spatial-scale turbulence that occurs at implosion and stagnation stages. Utilizing this axial magnetic field might allow for better control of precursor formation regimes as well [3,4,7] and may also be useful in studies on radiation pulse shaping [6]. The magnetic field configuration inside the DPWAsk load is much more complex than the one in a twisted cylindrical array because all DPWA-type loads have open magnetic configurations [4]. This fact hinders adequate numerical modeling of DPWAsk loads.

For calculations of the implosion characteristics of planar wire arrays, a new wire ablation dynamic model (WADM) [12] was developed and used in experimental research. A two-dimensional radiation magnetohydrodynamics (MHD) code [13] was applied to simulate the array implosions and stagnations of these Z-pinch experiments, and to reveal the pinch structure and effects related to anomalous plasma heating. The non-local-thermodynamic-equilibrium kinetic models (non-LTE) kinetic models developed at University of Nevada, Reno (UNR) (see, for example, [14]) allow detailed study of primary plasma parameters, such as temperature, electron density, and spatial and temporal gradients, via spectroscopic analysis.

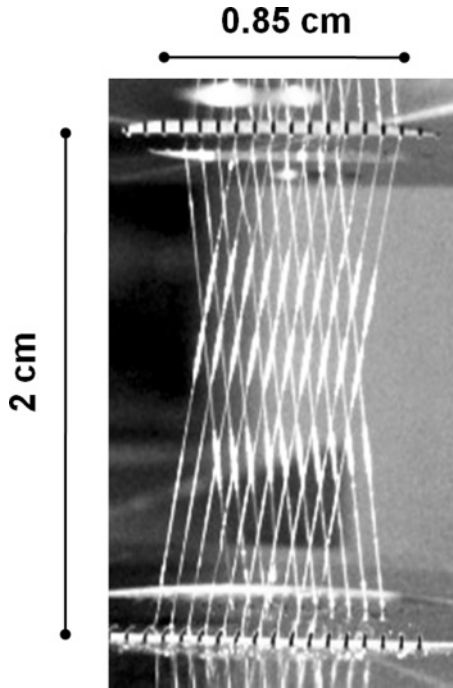


FIG. 1. Structure of DPWAsk (side view). The anode is at the top.

In this paper we describe the results of our research in the implosion dynamics and radiative properties of this new skewed planar wire array radiation source.

II. EXPERIMENTS ON IMPLOSION DYNAMICS AND RADIATIVE PROPERTIES OF DPWAS WITH SKEWED WIRES VERSUS CONVENTIONAL DPWAS

A. Diagnostics and preliminary experimental results

Experiments were performed on the 100 ns, 1.9 Ω impedance Zebra generator at UNR. The peak current during experiments was near 0.9 MA. The parameters of Z-pinch loads were optimized so that the array implosion times were within ± 10 –12 ns of the current maximum.

The DPWAsk load setup is shown in Fig. 1. The dimensions of a DPWAsk as well as a DPWA are the interwire gap d , the inter-row gap Δ , and the wire array width D . Also, the DPWAsk is characterized by the angle of wire inclination from central Z-pinch axis, α . The aspect ratio K is defined as the array width D divided by the inter-row gap Δ . The diagnostic setup included x-ray detectors (XRD), diamond photoconducting detectors (PCD), hard x-ray detectors (Si diodes), a Ni bolometer, a laser shadowgraphy system, an optical streak camera, a time-integrated and time-gated x-ray pinhole cameras, a spatially resolved time-integrated, and a spatially integrated, time-gated potassium hydrogen phthalate (KAP) convex crystal spectrometers. An 5 μm kimfoil-filtered XRD registered radiation with photons energy > 0.18 keV, and an 8 μm Be-filtered PCD registered radiation with energy > 0.75 keV. To study the time dependence of hard x-ray emission with photon energy > 9 keV, filtered fast Si diodes (AXUV-HS5) were used. A standard nickel bolometer was used for measurements of the total x-ray yields (0.01–6 keV). A visible-light optical streak camera with a spatial resolution

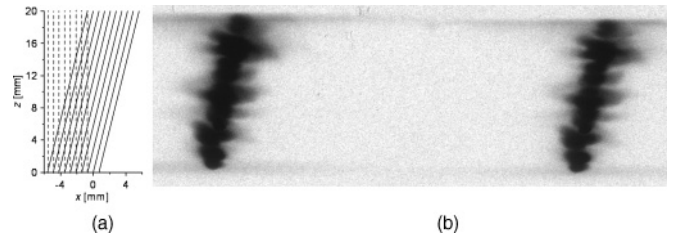


FIG. 2. (a) Initial positions of wires in SPWA with straight (dotted lines) and tilted wires (solid lines). The angle of wire inclination from the central Z-pinch axis is $\alpha = 8^\circ$. (b) Shot no. 1248. Implosion of planar wire with tilted wires (SPWA, W wires with diameter $\Phi_w = 5 \mu\text{m}$, number of wires $N_w = 24$, interwire gap $d = 0.5$ mm). Time-integrated x-ray images with energy filters > 3.3 keV, left; > 4 keV, right. Anode is at the top. Note that at stagnation, the angle of the plasma column with respect to the central Z-pinch axis is equal to the initial one, 8° .

0.35 mm was used to record plasma implosion trajectories as a continuous function of time. A laser probing system with time resolution 150 ps and spatial resolution 10 μm was used to generate shadowgraphy imaging.

The total energy of the electron beams in the created plasmas was measured using methods described in [15,16]. One method was based on estimating the total electron beam energy needed to generate the observed damage (crater) on the anode surface after the experiment. Another procedure was based on processing hard x-ray signals from calibrated Si diodes [17].

In earlier work we demonstrated that single planar arrays have implode even when the wires are not parallel to the central Z-pinch axis (see Fig. 2) with negligible variations in their plasma parameters. Because in the DPWA configuration each wire array implodes independently before stagnation [3,4], we expect that a similar cycle will also take place in the DPWAsk load.

In the first experiments with DPWAsks [4], the angle between wires in parallel rows was $2\alpha = 16^\circ$ ($\pm 8^\circ$ from the Z-pinch central axis) (Fig. 1). A more uniform plasma column was formed at stagnation than had been observed in conventional DPWAs with straight wires [4]. The total radiation yield E_T and power in the sub-keV spectral region for Al DPWAsks were similar to results from standard DPWAs, but the maximum electron temperature T_e was about 10% higher in the skewed configuration. Additionally, applications in radiation pulse shaping were demonstrated [4,6].

B. Experiments with Al and brass DPWAsks

In experiments with a standard DPWA (straight wires), a precursor has been observed with optical shadowgrams in the center of the inter-row gap with a “snake”-like structure that corresponds to $m = 0$ and $m = 1$ instabilities (Fig. 3) between two parallel double-layer structures at early times (40–60 ns before x-ray signal peak, Fig. 3) [3,7] that are dependent on the ablation properties of the wire material. These double-layer structures, according to the WADM modeling, represent the convergent region of the ablated plasma flows in open magnetic configurations [4]. Thus, experiments [3,4,7] and WADM simulations [12] suggest that in standard DPWA geometry, with either a high or low aspect ratio (K), precursor formation is a complex multistep dynamic

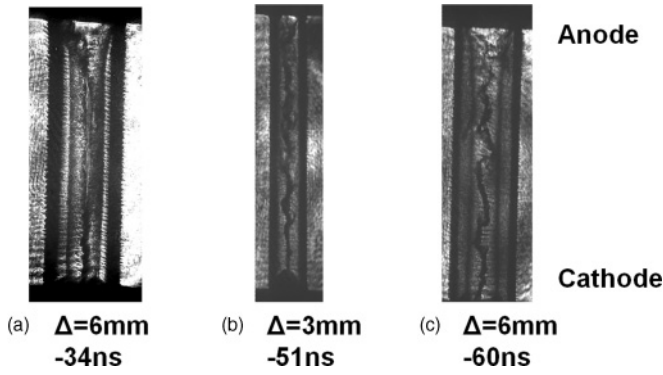


FIG. 3. Shadowgrams of standard DPWAs: (a) Shot no. 1789, Al, number of wires in each row $N_w = 10$, wire diameter $10 \mu\text{m}$. (b) Shot no. 1769, stainless steel. (c) Shot no. 1773, stainless steel. Number of wires in each row $N_w = 8$, wire diameter $10 \mu\text{m}$, $d = 0.7 \text{ mm}$. View is along wire row planes and perpendicular to wires. The time is in nanoseconds before x-ray peak.

process that is affected both by the array geometry and the ablation properties of the wire materials.

In more recent experiments with DPWAsks, the angle between wires in parallel rows was $2\alpha = 28^\circ (\pm 14^\circ \text{ to the Z-pinch central axis})$. The wires were made from materials with different ablation properties: Al and brass [14]. The application of both of these materials provides us with the possibility of measuring plasma electron temperature and density by x-ray spectroscopy [14]. WADM simulation suggests higher density and lower velocity for the ablated Al plasma, and lower density and higher velocity for the ablated flow of brass plasma [12].

The cascade-type implosion of DPWAsks starts (as in standard DPWAs [3,7]) from outside wires where current flows first [Figs. 4(a) and 4(b)]. The convergence regions of the inward flowing ablated plasma [Figs. 5(a) and 5(b)] produce a double-layer structure (as in standard DPWAs [7]), which can be observed on streak-camera images [Fig. 4(c)] at early times. The precursor structure appears several tens of nanoseconds before the primary x-ray signal peak. This smooth precursor structure, practically without instabilities, has also been seen clearly on shadowgrams of both Al [Fig. 5(a)] and brass

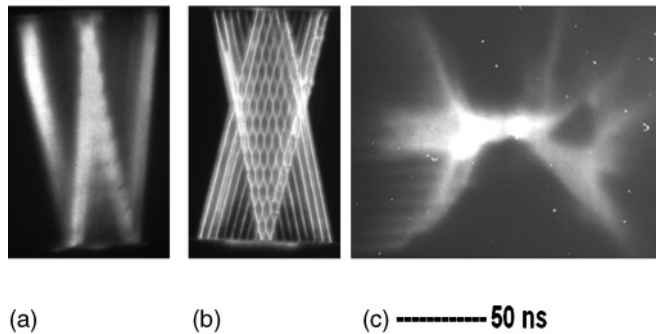


FIG. 4. Optical images of Al DPWAsk at (a) 90 ns and (b) 80 ns before x-ray signal peak. Frame duration is 2 ns. View is 45° (a) and 90° (b) to wire row planes. (c) Shot no. 1951. DPWAsk, $2\alpha = 28^\circ$, Al wires with diameter $\Phi_w = 10 \mu\text{m}$, number of wires in each row $N_w = 10$, interwire gap $d = 1 \text{ mm}$, and inter-row gap $\Delta = 6 \text{ mm}$. Optical streak-camera image with resolution 4 ns also shown. View is 45° to wire row planes.

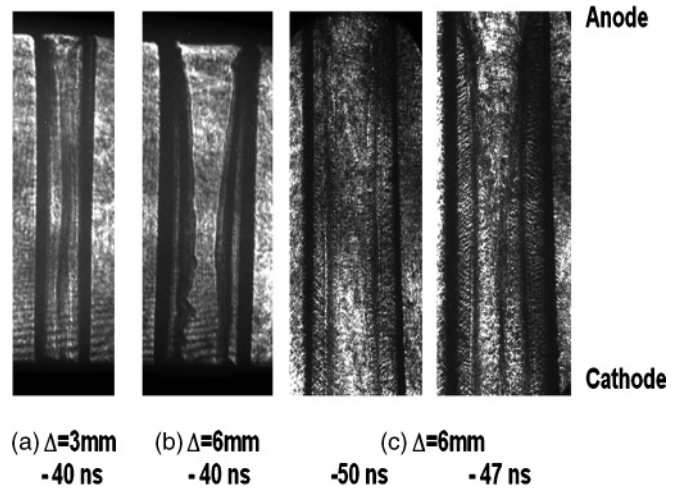


FIG. 5. Shadowgrams of Al DPWAsk; observation is along wire row planes. (a) Shot no. 1779 and (b) shot no. 1778: number of wires in each row $N_w = 10$, wire diameter $10 \mu\text{m}$, $d = 0.7 \text{ mm}$. (c) Shot no. 2149: number of wires in each row $N_w = 8$, wire diameter $12.7 \mu\text{m}$ (in this picture the region from the anode to the middle of the anode-cathode gap is seen), $d = 1 \text{ mm}$. The time is in nanoseconds prior to x-ray peak.

DPWAsk [Fig. 6(a)] with high aspect ratio ($\Delta = 3 \text{ mm}$, $K = 2.1$); the $m = 0$ instability is significantly reduced and the $m = 1$ instability is practically absent. Another interesting feature is the observed turbulent zone near the anode that occurs in all DPWA and DPWAsk loads. For low aspect ratio ($\Delta = 6 \text{ mm}$, $K = 1.05$) DPWAsk Al [Figs. 5(b) and 5(c)] and brass [Fig. 6(b)] loads, a process of smooth precursor formation was also observed, but the structure of the precursor

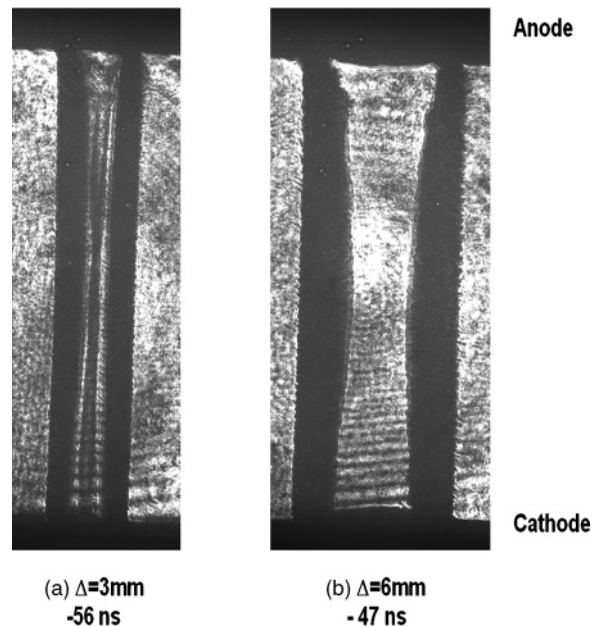


FIG. 6. Shadowgrams of brass (30% Zn, 70% Cu) DPWAsk: (a) Shot no. 1784, (b) shot no. 1786. Number of wires in each row $N_w = 10$, wire diameter $7.62 \mu\text{m}$, and $d = 0.7 \text{ mm}$. View is along wire row planes and perpendicular to wires. The time is in nanoseconds prior to x-ray peak.

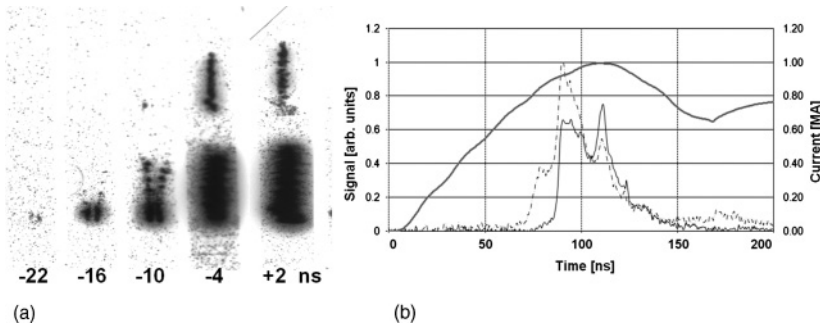


FIG. 7. Shot no.1783: Al DPWAsk, $\Delta = 6$ mm, $2\alpha = 28^\circ$, $N_w = 10$, wire diameter $\Phi_w = 10 \mu\text{m}$, $d = 0.7$ mm. (a) X-ray time-gated images at the top >3 keV and at the bottom >1 keV. Frame duration 3 ns and interframe interval 6 ns. Direction of view is 45° to wire row planes. The anode is at the bottom. The time is in nanoseconds prior to the x-ray peak. (b) XRD sub-keV signal (dotted line), PCD keV signal (thin black line), and current (thick black line) vs time.

was much less pronounced compared to high aspect ratio DPWAsks.

All these facts indicate that MRT instabilities in precursor plasmas were suppressed by the axial magnetic field B_z of the DPWAsk (Figs. 5 and 6). In particular, the axial magnetic field suppressed both $m = 0$ (sausagelike) and $m = 1$ (snakelike) instability modes, as the precursor column was uniform in these experiments (Figs. 5 and 6). Later (15–20 ns before stagnation), the plasma became hotter and appeared on images recording energies >1 keV [Fig. 7(a)]. As in a standard DPWA, the formations of secondary double precursor columns occurred in later time and consisted of bright spots [3]. However, these columns were not parallel to each other (V-shaped cross-column structure is seen at an angle $<45^\circ$ to wire row planes), which is different from secondary precursor formations observed in loads with parallel plasma columns [3] in a standard DPWA. Note that in the DPWAsk load, the formation of secondary double precursor plasma columns starts much earlier (~ 20 – 25 ns before the x-ray peak signal) than in a standard DPWA (10–15 ns) [3].

After the appearance of the secondary precursor columns they begin to merge (from the center of the anode-cathode gap) into the final stagnated Z-pinch plasma column that radiates the main x-ray pulse. The time of this merging is strongly correlated with the formation of the sub-keV prepulse, which is clearly observed from x-ray sub-keV (XRD) signals [Fig. 7(b), dotted line]. According to the WADM simulations, the generation of the small sub-keV prepulse can be explained by the thermalization of the kinetic plasma energy due to the off-axial convergence of plasma remnants of each wire plane. Often, this time also corresponds to the formation of secondary precursor double-column structures on pinhole x-ray images [3], which is significantly modified by DPWAsk geometry [inclined or “cross-column” structure, as in Fig. 7(a)]. According to the WADM modeling, the time between off-axial plasma convergence and the final plasma merging at the array center is typically 5–10 ns. Also, as was mentioned earlier, secondary precursor plasma double-column formation starts much earlier (~ 20 – 25 ns before x-ray peak signal) in a DPWAsk load than in a standard DPWA (10–15 ns).

By controlling these time intervals, the position of the x-ray prepulse with respect to the main x-ray burst can be shifted. The possibility of prediction and control of prepulse times in DPWAsks opens a way to more effectively shape radiation pulses [including the formation of a sub-keV step pulse that appears at the foot of the main pulse [6] and the sharp prepulse that forms before the main pulse; Fig. 7(b), dotted line] than

with a standard DPWA by changing the DPWAsk geometry and wire materials.

The total radiation yield E_T and power from the DPWAsks in the sub-keV spectral region were 10–15 % smaller compared to standard DPWA results. A possible explanation of this decrease can be provided by the fact that the DPWAsk load is not a symmetrical load along its z axis, contrary to the standard DPWA. Therefore, it is likely that asymmetric implosion of the DPWAsk is causing the observed decrease of the radiation yield in the sub-keV spectral range. At the same time, the stabilization effect due to the induced axial magnetic field should increase the conversion efficiency of the electromagnetic energy into the radiation. Thus, the optimization of DPWAsk loads seems to be an important research direction for the near future.

The spatial gradients of electron temperatures (T_e) and density (N_e) of Al and brass DPWAsk plasmas were determined from non-LTE modeling [14,18] of axially resolved time-integrated spectra (Fig. 8). In particular, these parameters were determined from modeling of K -shell Mg (5% concentration in alloy Al 5056) and L -shell Cu and Zn features in spatially resolved time-integrated spectra (Figs. 8–10). The T_e and N_e spatial distribution for Al and brass DPWAsks were found to be drastically different. The difference in x-ray radiation and spectroscopy measurements are due to the fact that the modeled spectral region represents two different types of radiation: K -shell radiation of Al and L -shell radiation of Cu and Zn radiation, which have, in general, different radiative properties that were studied and described elsewhere (see, for example, [18,19]).

Two Al 5056 DPWAsk configurations were investigated, one with $2\alpha = 16^\circ$ (Fig. 8) and another with $2\alpha = 28^\circ$ (Fig. 9). The total radiation yield was near 12 kJ and implosion time was between 100 and 110 ns for both configurations. Electron temperatures (T_e) up to 410 eV and densities (N_e) up to $9 \times 10^{19} \text{ cm}^{-3}$ were observed for the array with $2\alpha = 16^\circ$ (Fig. 8). In comparison, the modeling of plasmas from the array with $2\alpha = 28^\circ$ (Fig. 9) has been shown to have a lower maximum T_e of about 380 eV and somewhat higher N_e of $1.4 \times 10^{20} \text{ cm}^{-3}$. Thus, it has been deduced that Al DPWAsk plasmas are characterized by higher T_e and slightly lower N_e than that of a standard Al DPWA ($T_e \sim 350$ eV and $N_e \sim 2 \times 10^{20} \text{ cm}^{-3}$) [3]. It is important to emphasize that both T_e and N_e in DPWAsk Al plasmas express strong nonuniformities and gradients between the anode and cathode in a large range of plasma parameters: $T_e \sim 355$ – 405 eV and $N_e \sim 5 \times 10^{19} \text{ cm}^{-3}$ to $9 \times 10^{19} \text{ cm}^{-3}$ for $2\alpha = 16^\circ$, and $T_e \sim 320$ – 380 eV, $N_e \sim 5 \times 10^{19} \text{ cm}^{-3}$ to $1.4 \times 10^{20} \text{ cm}^{-3}$ for $2\alpha = 28^\circ$.

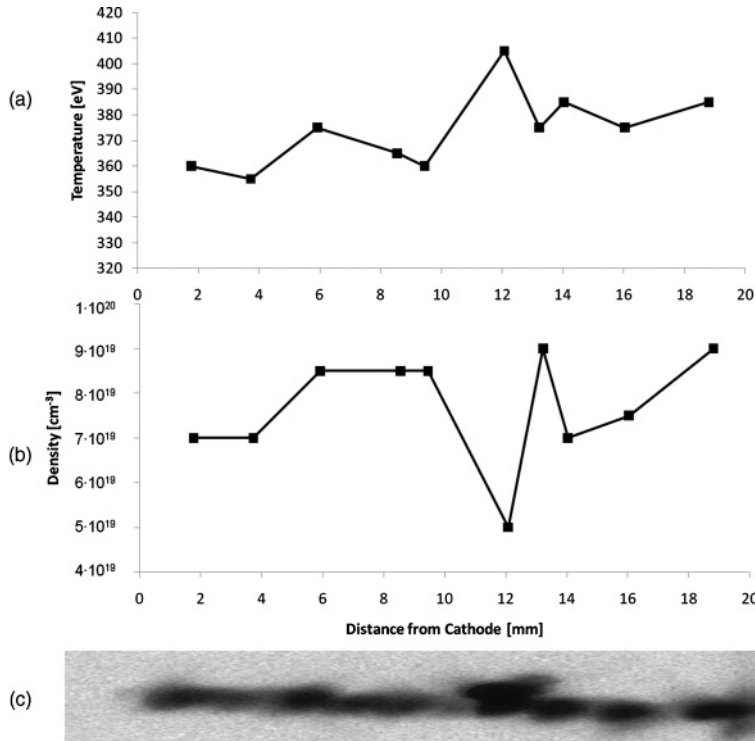


FIG. 8. Experimental dependence of electron temperature T_e and density N_e on the distance from the cathode for shot no. 2150, Al (5056) DPWAsk, $2\alpha = 16^\circ$, wires with diameter $\Phi = 12.7 \mu\text{m}$, number of wires in each row $N_w = 8$, interwire gap $d = 1 \text{ mm}$, inter-row gap $\Delta = 6 \text{ mm}$. At the bottom is a pinhole image of the plasma in the spectral region of wavelengths $>4.4 \text{ \AA}$ (image was compressed in a direction perpendicular to the Z-pinch axis).

At the same time, the strong inverse correlation between T_e and N_e was observed between the anode-cathode gap; the maximum T_e corresponds to the minimum N_e for both array configurations. The effects due to Z-pinch nonuniformity at the stagnation stage have been discussed in [16]. It was shown that nonuniform Z-pinch plasma at near equilibrium with the magnetic field has a higher T_e in the regions with lower N_e and vice versa. In both Figs. 8 and 9 the location of the peak of electron temperature corresponds to the location of the plasma region with the lowest value of electron density. Thus, time-integrated images (in the spectral region $>4.4 \text{ \AA}$) suggest

that at stagnation Al DPWAsk plasma has nonuniformities as a result of the growth of $m = 0$ instability modes.

In brass DPWAsks, electron temperatures T_e showed sharper increases near the anode and decreases toward the cathode compared to Al DPWAsks. Two brass DPWAsk configurations with $2\alpha = 28^\circ$ were investigated, one with inter-row gap $\Delta = 3 \text{ mm}$ and another with $\Delta = 6 \text{ mm}$ (Fig. 10). The total radiation yield was near 26 kJ for both configurations. In a standard brass DPWA, T_e showed monotonic behavior with temperature increases at the anode (450 eV) and decreases toward the cathode (400 eV) [18], which is opposite of what

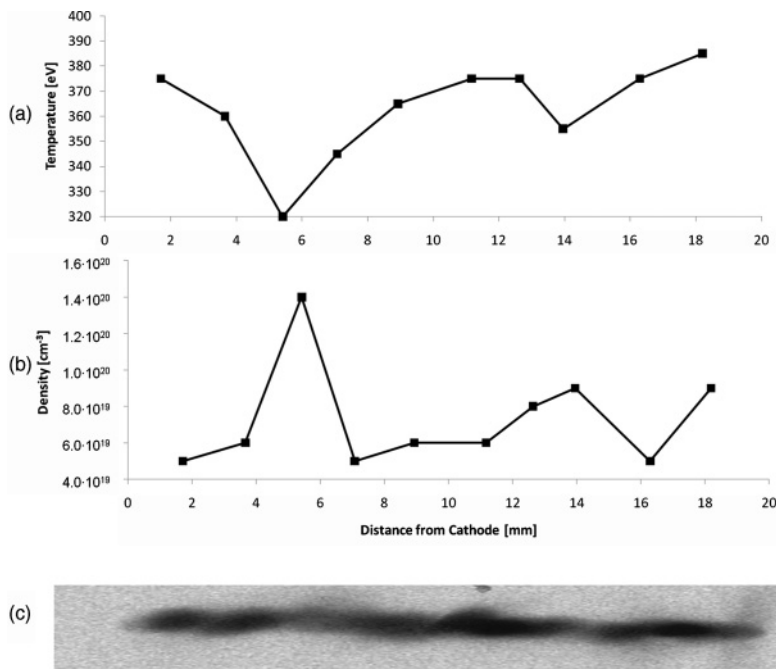


FIG. 9. Experimental dependence of electron temperature T_e and density N_e on the distance from the cathode for shot no. 2148, Al (5056) DPWAsk, $2\alpha = 28^\circ$, wires with diameter $\Phi_w = 10 \mu\text{m}$, number of wires in each row $N_w = 10$, interwire gap $d = 1 \text{ mm}$, inter-row gap $\Delta = 6 \text{ mm}$. At the bottom is a pinhole image of the plasma in the spectral region of wavelength $>4.4 \text{ \AA}$ (image was compressed in a direction perpendicular to the Z-pinch axis).

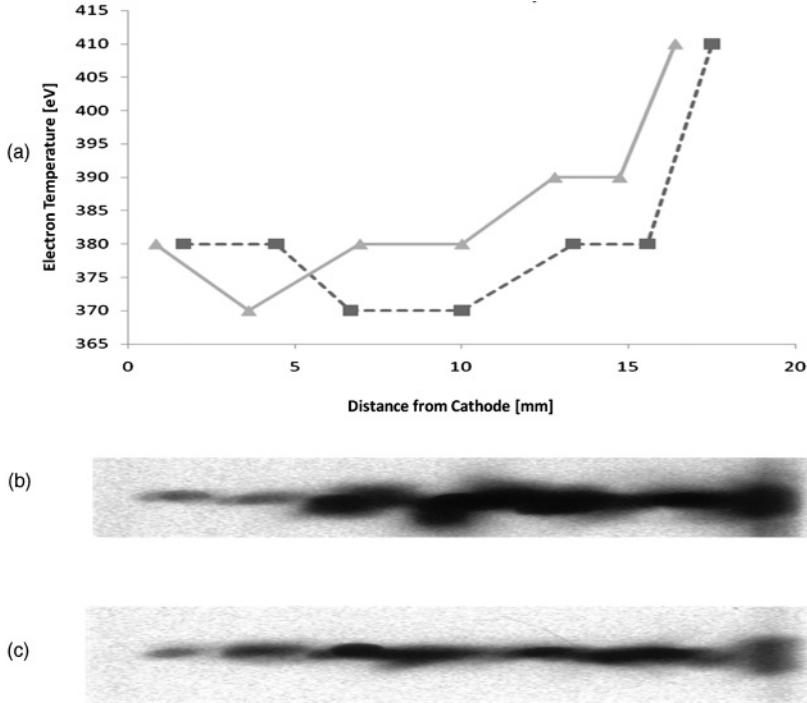


FIG. 10. Experimental dependence of electron temperature T_e on the distance from the cathode for brass DPWAsk, $2\alpha = 28^\circ$, wires with diameter $\Phi_w = 7.62 \mu\text{m}$, number of wires in each row $N_w = 10$, interwire gap $d = 0.7 \text{ mm}$, inter-row gap $\Delta = 3 \text{ mm}$ in shot no.1784 (■), and $\Delta = 6 \text{ mm}$ in shot no.1786 (▲). Below are pinhole images of the plasmas in the spectral region with wavelengths $>4.4 \text{ \AA}$: shot no. 1784 at the top, shot no. 1786 at the bottom (images were compressed in a direction perpendicular to the Z-pinch axis).

was observed in DPWAsks with T_e having maximums near the anode (410 eV), minimums (about 370–380 eV) in the middle anode-cathode gap, and a slight increase near the cathode ($\sim 380 \text{ eV}$). Thus, it was determined that the T_e of brass DPWAsks was generally lower (by 30–40 eV) than in a standard brass DPWA [18] (Fig. 10), but DPWAsks with $\Delta = 6 \text{ mm}$ have demonstrated somewhat higher T_e (ΔT was more than 10 eV) than in arrays with $\Delta = 3 \text{ mm}$. The N_e in DPWAsks expresses almost uniform behavior between the anode and cathode ($N_e \sim 5 \times 10^{19} \text{ cm}^{-3}$). At the same time, that value was higher than in standard brass DPWA [18] by a factor of 5.

The main differences in plasma formations between DPWAsks and standard DPWAs were found at early times (several nanoseconds before the x-ray peak) when precursors were formed; more uniform precursors were observed for DPWAsks (Figs. 3, 5, and 6). The structure of DPWAsk plasma columns at stagnation with a large number of bright spot clusters positioned along the Z-pinch axis look similar to a those of a standard DPWA, but with an important difference: DPWAsk columns do not have large regions devoid of bright spots at stagnation, as was observed for standard DPWAs. The axial magnetic field suppressed both $m = 0$ and $m = 1$ mode instabilities at the precursor formation stage and $m = 1$ mode instability at the stagnation phase. However, the $m = 0$ instability mode is the most likely to affect the Z-pinch stagnation stage, creating plasma nonuniformities along the pinch axis, according to the analysis of spatially resolved spectroscopic modeling.

III. DISCUSSION

In a conventional geometry of a DPWA load (with straight wires) the dynamics of the inward flows of the ablated plasmas as well as the array implosion itself are governed by the magnetic pressure, created by the azimuthal component of the

magnetic field B_θ . Interaction of B_θ with the axially directed currents in plasmas is the result of the Lorentz $\mathbf{j} \times \mathbf{B}$ force, which is directed toward the geometrical center of the array, causing the inward acceleration of the array plasma [4,8,14].

This dynamic picture may change due to the presence of an axial magnetic field component B_z . The interaction of an axial magnetic field with tilted plasma currents can be responsible for the generation of a Lorentz force component that is directed from the array center toward the load periphery. Thus, the magnetic field pressure induced by its axial component, which increases faster than the azimuthal component while the plasma column is compressed ($B_z \sim 1/r^2$, while $B_\theta \sim 1/r$), generally counteracts the precursor formation and array implosion. In the extreme case, the so-called “force-free” configuration can be created where electrical current flows along the magnetic field, neutralizing the Lorentz $\mathbf{j} \times \mathbf{B}$ force and putting the system into quasiequilibrium. The detailed theory of the nearly force-free configuration and its stabilities was developed in works by Shafranov, Morozov, and Taylor (see, for example, [20–22]).

The magnetic field distribution in the DPWAsk load configuration, with schematics as shown in Fig. 11(a), is much more complex compared to the magnetic field of a traditional plasma column. The main reason is that the DPWA load represents open magnetic field geometry [4], where the global magnetic field is allowed to penetrate toward the array center through the gaps between the wire planes. One of the ways to calculate the magnetic field distribution is, for example, to employ the Biot-Savart law

$$\mathbf{B} = \frac{\mu_0}{4\pi} \sum_n \int \frac{I_n d\mathbf{l}_n \times \mathbf{r}_n}{r_n^3}, \quad (1)$$

where I_n is the current through the n th wire, $d\mathbf{l}_n$ is the differential vector of the n th wire directed along the current, and \mathbf{r}_n is the full displacement vector from the wire element to

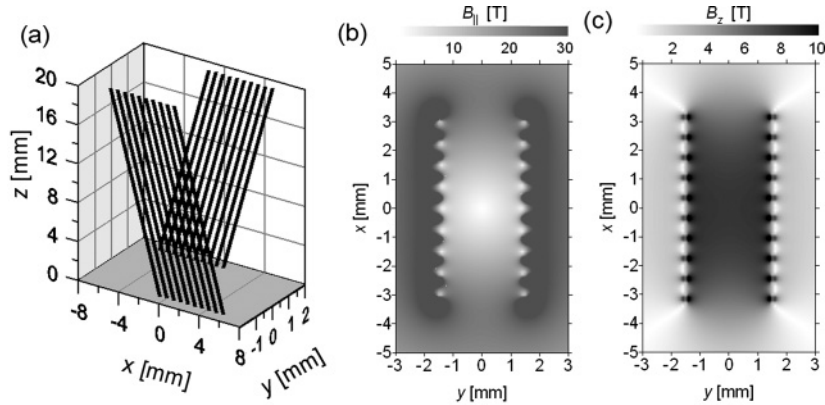


FIG. 11. (a) Initial wire positions in a DPWAsk load (total number of wires $N_w = 2 \times 10$, inter-row gap $\Delta = 3$ mm, full skew angle $2\alpha = 28^\circ$) shown with Cartesian coordinates. [(b) and (c)] Two-dimensional (x,y) distributions of the absolute values of the longitudinal $B_{||} = \sqrt{B_x^2 + B_y^2}$ and axial B_z magnetic field components, calculated by Eq. (1) in the plane $z = 10$ mm [with respect to plot (a)]. Intensities of the magnetic field components are calculated for total current $I = 0.5$ MA (middle of the current rise time).

the point at which the field is being computed. The distributions of the magnetic field components, calculated according to Eq. (1), in the middle plane of the wire array are presented in Fig. 11. The general features of the magnetic field distribution in the solenoid still hold for the skewed wire DPWA load; the longitudinal magnetic field component $B_{||}$ is strong outside of the array and almost vanishes at the array center, while the axial magnetic field component is strong at the inside of the array

A prediction made using WADM of the position of the secondary precursor plasma columns (Fig. 12) was found to be in good correlation with experimental observations before stagnation [Fig. 7(a)]. Three-dimensional MHD simulations of mutual dynamics of two Z pinches that highlight the wire array ablation dynamics have been performed in [23] for a typical x-pinch geometry (two wires carrying current and crossing at some point at a 90° angle, as shown in Fig. 13). It was shown [23] that a force-free configuration is formed in the vicinity of the x-pinch crossing point. As we can see in Fig. 13(a), initially two current streams are directed along each Z pinch (wire), while the magnetic field is almost entirely azimuthal and spirals around these currents. Figure 13(b) shows the results of a simulation of plasma dynamics at a later stage. As we can see, at that moment two current streams have merged into a single

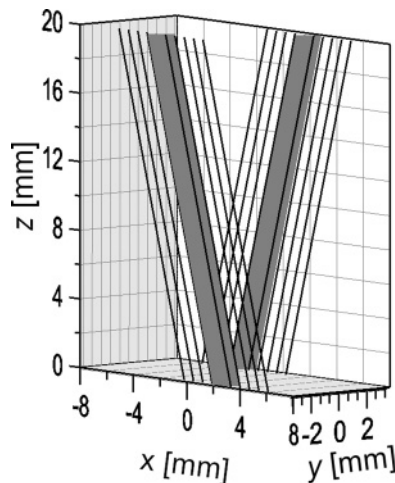


FIG. 12. Shot no. 1780: WADM prediction of positions of secondary precursor plasma columns (shown in gray) 15 ns before stagnation (original wire positions shown as solid black lines). Direction of view is 45° to wire row plane. The anode is at the bottom.

stream directed between the initial positions of the wires, while the magnetic field reconfigures in the way that it is directed mostly along the current (analogous of the axial component of the magnetic field in standard wire array configurations). In this case a force-free configuration is formed. This simulation was kindly made for us by Dr. J. Huba from Naval Research Laboratory.

Some additional evidence of the enhanced stabilization of Z pinches, created by the implosion of DPWAsk load, can be supported by the experimental observations of the increased electron beam generation by the DPWAsk loads versus conventional straight DPWA loads. Favorable conditions for the electron beam generation for various wire array configurations have been discussed in [16,17]. One of the possible explanations for the increased amount of total electron beam energy in DPWAsk configurations could be explained by increased axial nonuniformity ($m = 0$ “sausage”-type instability modes) of the resultant Z pinch due to initial load

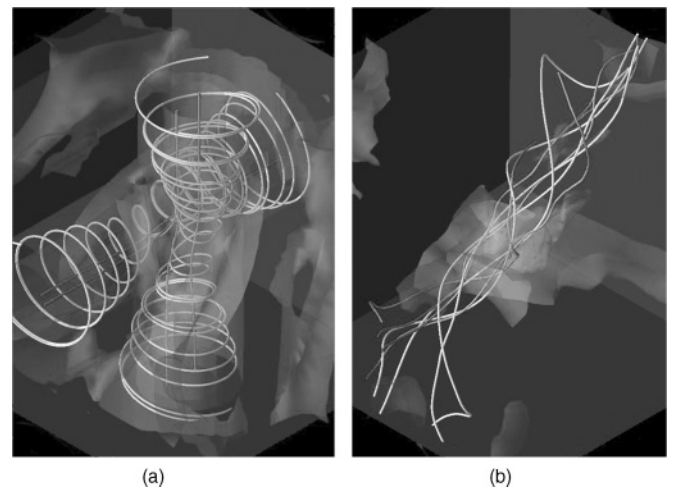


FIG. 13. 3D MHD simulation of plasma and magnetic field dynamics of Z pinch in x-pinch configuration. The direction of current flow and the magnetic field force lines are presented by the gray and white lines, respectively. (a) At the initial moment the electric current flows along x-pinch limbs (double gray lines inside spirals), which are at a right angle from each other. The magnetic field at this moment is mostly azimuthal (magnetic field lines are the white spiral lines around the currents). (b) After some time a force-free configuration is formed with currents and magnetic field lines parallel to each other.

asymmetry along the array axis z . However, this hypothesis is not strongly supported by the spectroscopic modeling (see, for example, the data in Figs. 8 and 9), which does not reveal significant changes of the electron density along the pinch axis. Another explanation could be the enhanced stabilization of the $m = 1$ snake-type instability modes, which can increase the compactness of the final Z pinch and generate more intense components of the axial electric field, as well as produce electron beams of higher intensity. This hypothesis is supported by the experimental data showing the stabilization of $m = 1$ modes during the stage of precursor formation (compare the laser shadow images in Figs. 3 and 5). It is likely that the same stabilization mechanism is affecting Z -pinch formation at the end of the implosion stage of the DPWAsk loads.

IV. CONCLUSION

In conclusion, we have studied the influence of an induced axial magnetic field on the plasma dynamics and radiative characteristics of Z pinches. The axial magnetic field was induced using a new Z -pinch load: double planar wire arrays with skewed wires (DPWAsks), which represent the planar wire array with open magnetic configuration. The possibility of achieving better control of x-ray radiation output in DPWAsks compared to a standard DPWA with straight wires was demonstrated.

The implosion dynamics of DPWAsk plasmas is a complex multistep process that is affected both by the array geometry and the ablation properties of the wire materials. The axial magnetic field, generated by skewed wires, suppressed Z -pinch plasma MRT instabilities (with $m = 0$ and $m = 1$ instability modes) and led to the formation of more uniform precursor plasma columns at early time than compared to a standard DPWA. The suppression of MRT in the formation of a sub-keV prepulse before the

main x-ray peak enables improved radiation pulse shaping, a key requirement for ICF applications. The possibility of prediction and control of this prepulse appearance opens a new way to improve radiation pulse shaping through changing DPWAsk geometry and wire material. This is important for ICF applications, despite the fact that the DPWAsk total radiation yield E_T was 10–15 % lower than from a standard DPWA.

Also, the influence of the initial axial magnetic field on the structure of DPWAsk plasma columns at stagnation was manifested through the formation of more uniform DPWAsk plasma columns (without $m = 1$ instability mode) than from a standard DPWA.

A significant difference in plasma parameters along the cathode-anode gap was observed for all DPWAsks made from low atomic number (Z) wires (Al) and mid- Z wires (brass). The Al DPWAsk plasma was characterized by higher T_e and lower N_e in comparison with plasma from a standard Al DPWA. Both T_e and N_e in DPWAsk Al plasma express strong nonuniformities between the anode and cathode. In brass DPWAsks, T_e showed behavior with increases near the anode and decreases toward the cathode that was more pronounced than in Al DPWAsks. The maximum T_e of brass DPWAsk plasmas was slightly lower (by 10%) than in standard brass DPWAs, and N_e was nearly constant along the cathode-anode gap and was several times higher than in standard brass DPWAs.

ACKNOWLEDGMENTS

The authors would like to express gratitude to the NTF technical team, B. LeGalloudec, A. Astanovitsky, V. Nalajala, S. Batie, and O. Dmitriev, for their great work in Zebra operations and data collection during these experiments. Work was supported by the DOE/NNSA Cooperative agreements DE-FC52-06NA27588, DE-FC52-06NA27586, and in part by DE-FC52-06NA27616.

-
- [1] C. Deeney, M. R. Douglas, R. B. Spielman, T. J. Nash, D. L. Peterson, P. L'Eplattenier, G. A. Chandler, J. F. Seamen, and K. W. Struve, *Phys. Rev. Lett.* **81**, 4883 (1998). PRLTAO 0031-9007
 - [2] V. L. Kantsyrev *et al.*, *IEEE Trans. Plasma Sci.* **34**, 2295 (2006); *High Energy Density Physics* **3**, 136 (2007).
 - [3] V. L. Kantsyrev *et al.*, *Phys. Plasmas* **15**, 030704 (2008).
 - [4] V. L. Kantsyrev *et al.*, *High Energy Density Phys.* **5**, 115 (2009).
 - [5] B. Jones *et al.*, *Phys. Rev. Lett.* **104**, 125001 (2010).
 - [6] V. L. Kantsyrev *et al.*, *J. Phys.: Conf. Ser.* **244**, 032030 (2010).
 - [7] K. M. Williamson *et al.*, *Phys. Plasmas* **17**, 112705 (2010).
 - [8] S. Chandrasekhar, *Hydrodynamic and Hydromagnetic Stability* (Clarendon, Oxford, 1961).
 - [9] L. Rudakov and R. Sudan, *Phys. Rep.* **283**, 253 (1997).
 - [10] N. B. Volkov *et al.*, *Laser Part. Beams* **19**, 451 (2001).
 - [11] Lebedev *et al.*, *Plasma Phys. Controlled Fusion* **47**, B465 (2005).
 - [12] A. A. Esaulov *et al.*, *High Energy Density Phys.* **5**, 166 (2009).
 - [13] A. S. Chuvatin *et al.*, *IEEE Trans. Plasma Sci.* **33**, 739 (2005).
 - [14] A. S. Safronova *et al.*, *Phys. Plasmas* **15**, 033302 (2008).
 - [15] V. Kantsyrev *et al.*, *Phys. Plasmas* **10**, 2519 (2003).
 - [16] I. K. Shrestha *et al.*, *IEEE Trans. Plasma Sci.* **34**, 658 (2010).
 - [17] I. K. Shrestha, Ph.D. Dissertation, *University of Nevada, Reno*, 2010.
 - [18] N. D. Ouart *et al.*, *IEEE Trans. Plasma Sci.* **34**, 63 (2010).
 - [19] A. S. Safronova *et al.*, *High Energy Density Phys.* **3**, 237 (2007).
 - [20] J. B. Taylor, *Phys. Fluids* **4**, 1142 (1961).
 - [21] V. D. Shafranov, in *Reviews of Plasma Physics*, edited by M. A. Leontovich (Consultant Bureau, New York, 1966), Vol. 2, p. 103.
 - [22] A. I. Morozov and L. S. Solov'ev, in *Reviews of Plasma Physics*, edited by M. A. Leontovich (Consultant Bureau, New York, 1966), Vol. 2, p. 201.
 - [23] J. D. Huba, L. I. Rudakov, and V. I. Sotnikov, *3D Dynamics of X- and Z-Pinches*, Book of Abstracts of IEEE 2005 International Conference (June 20–23, 2005, Monterey, CA), p. 308.